
Nanodust in the Interstellar Medium in Comparison to the Solar System

Aigen Li and Ingrid Mann

¹ Department of Physics and Astronomy, University of Missouri, Columbia, MO 65211, USA; LiA@missouri.edu

² Belgian Institute for Space Aeronomy, B-1180 Brussels, Belgium; ingrid.mann@aeronomie.be

Summary. Nanodust, which undergoes stochastic heating by single starlight photons in the interstellar medium, ranges from angstrom-sized large molecules containing tens to thousands of atoms (e.g. polycyclic aromatic hydrocarbon molecules) to grains of a couple tens of nanometers. The presence of nanograins in astrophysical environments has been revealed by a variety of interstellar phenomena: the optical luminescence, the near- and mid-infrared emission, the Galactic foreground microwave emission, and the ultraviolet extinction which are ubiquitously seen in the interstellar medium of the Milky Way and beyond. Nanograins (e.g. nanodiamonds) have also been identified as presolar in primitive meteorites based on their isotopically anomalous composition. Considering the very processes that lead to the detection of nanodust in the ISM for the nanodust in the solar system shows that the observation of solar system nanodust by these processes is less likely.

1 Introduction: The Interstellar Medium and Nanodust

The stars in our Galaxy, the Milky Way, are far apart (e.g. the nearest star, Proxima Centauri, is at a distance of $\sim 2.67 \times 10^5$ AU from the Sun; $1 \text{ AU} \approx 1.496 \times 10^{13}$ cm). The space between stars contains gaseous ions, atoms, molecules and solid dust grains (i.e. the interstellar medium, ISM). With a mean number density of $\sim 1 \text{ H-atom/cm}^3$ it is more empty than the best vacuum (which has a density of $\sim 10^3 \text{ molecules/cm}^3$) that can be created on Earth. The gas and dust of the ISM makes up $\sim 10\%$ of the total mass of the visible matter in the present-day Milky Way.³ The bulk of the heavy elements, including most of the interstellar silicon, magnesium, iron and a large fraction of the interstellar carbon, are depleted from the gas phase and form submicron-sized grains, which make up $\sim 1\%$ of the total mass of the ISM. In a spiral galaxy like the Milky Way, most of the interstellar dust and gas are concentrated in its spiral arms and a relatively thin gaseous disk of a thickness of a few hundred parsecs (pc ; $1 \text{ pc} \approx 3.086 \times 10^{18}$ cm).

³ This mass fraction is much higher for galaxies at early times (since the ISM is gradually consumed by star formation as galaxies evolve) and much lower ($\sim 0.1\%$) for elliptical galaxies.

The ISM plays a crucial role in galaxy evolution: New stars form out of dusty molecular clouds which present a dense phase of the ISM while stars in late stage of evolution return gas and newly formed dust to the ISM (either through stellar winds or supernova explosions). The astrophysics of the ISM, from the thermodynamics and chemistry of the gas to the dynamics of star formation is strongly influenced by the presence of the dust.

The existence of small solid dust grains in interstellar space was established in 1930 when Trumpler showed that the stars in distant open clusters appear fainter than could be accounted for just by the inverse square law, and many stars in the galactic plane appear redder than expected from their spectral types; he interpreted these observations in terms of interstellar extinction and selective absorption (i.e. reddening) caused by “fine cosmic dust particles of various sizes” (Trumpler 1930). In 1956 John Platt suggested that very small grains or large molecules of less than 1 nm in radius could grow in the ISM by random accretion from interstellar gas and could be responsible for the interstellar extinction. Today the presence of nanodust in the ISM is generally accepted, but there are still uncertainties in interpreting observations. The discussion in this chapter will focus on the ultrasmall, nano-sized interstellar grains. By nano-sized grains, or nanodust we mean grains with a spherical radius of $a \lesssim 10\text{--}20$ nm which undergo stochastic heating in the Galactic ISM (Draine & Li 2001, Li 2004).

For a long time most of our knowledge about interstellar dust was derived from interstellar extinction and reddening, and to a lesser degree from interstellar polarization (which is caused by preferential extinction of one linear polarization over another by aligned nonspherical dust) and we will discuss this in the following section (2). Infrared observations from satellites started in the 1980s and allowed for observing the emission from interstellar dust. The observations indicate the presence of stochastically heated nanodust and emitting polycyclic aromatic hydrocarbon molecules (PAHs) discussed in section (3). Other observational results are also explained with the presence of nanodust: the microwave emission of rotationally excited nanodust (section 4), the photoluminescence of nanodust (section 5), and indirect evidence comes from the photoelectric heating of interstellar gas (section 6). Another population of nanodust are presolar nanograins that are identified in primitive meteorites and interplanetary dust and were present in the ISM at the time for the formation of the solar system (section 7). Based on the different processes that provide evidence for the existences of nanodust in the ISM we then make a comparison to the nanodust in the solar system (section 8) and end with a conclusion. The interstellar extinction and the stochastic heating process are elaborated in the appendix.

2 The Interstellar Extinction

For the ISM in the solar neighbourhood (i.e. a few kiloparsecs from the Sun and within ~ 100 pc of the galactic plane), the mean visual extinction per unit path-length of $\langle A_V/L \rangle \approx 1.8 \text{ mag kpc}^{-1}$ has long been determined quite accurately (e.g. see Kapteyn 1904). The wavelength-dependence of extinction – the interstellar extinction curve increases from red to blue, so that the light reaching us from the stars is “reddened” owing to greater attenuation of the blue light. The Galactic

interstellar extinction curves have now been measured for various sightlines over a wide wavelength range ($0.1 \mu\text{m} \leq \lambda \leq 20 \mu\text{m}$).

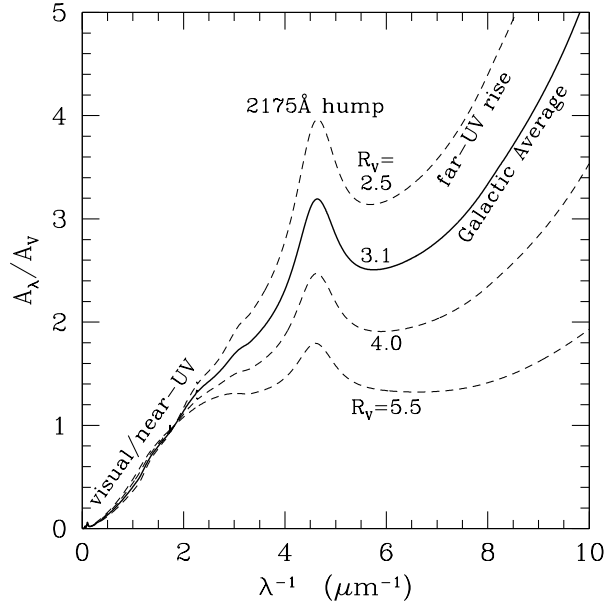


Fig. 1. Interstellar extinction curves of the Milky Way ($R_V = 2.5, 3.1, 4.0, 5.5$). There exist considerable regional variations in the Galactic optical/UV extinction curves, as characterized by the total-to-selective extinction ratio R_V , indicating that dust grains on different sightlines have different size distributions.

Although the extinction curves vary in shape from one line of sight to another, they do exhibit some common appearance (see Fig. 1). The extinction curves are plotted as A_λ/A_V , where A_λ is the extinction at wavelength λ measured in astronomical magnitudes and typically given relative to the extinction A_V in the visible wavelength band. The extinction curves shown vs. inverse wavelength λ^{-1} rise almost linearly from the near-infrared (IR) to the near-ultraviolet (UV), with a broad absorption bump at about $\lambda^{-1} \approx 4.6 \mu\text{m}^{-1}$ ($\lambda \approx 2175 \text{ \AA}$) and followed by a steep rise into the far-UV at $\lambda^{-1} \approx 10 \mu\text{m}^{-1}$, the shortest wavelength at which the extinction has been measured.

In the wavelength range of $0.125 \mu\text{m} \lesssim \lambda \lesssim 3.5 \mu\text{m}$, the Galactic extinction curves can be approximated by an analytical formula involving only one free parameter: the total-to-selective extinction ratio, R_V (Cardelli et al. 1989, see appendix). The sightlines through diffuse gas in the Milky Way have $R_V \approx 3.1$ as an average value, but there are considerable regional variations and also the strength and width of the 2175 \AA extinction bump vary markedly in the ISM (see Xiang et al. (2011) and references therein). Lower-density regions have a smaller R_V , a stronger 2175 \AA bump and a steeper far-UV rise at $\lambda^{-1} > 4 \mu\text{m}^{-1}$, while denser regions have a larger R_V , a weaker 2175 \AA bump and a flatter far-UV rise.

The exact nature of the carrier of this bump remains unknown since its first discovery nearly half a century ago (Stecher 1965). It has been postulated to be nano carbon particles (e.g. Duley & Seahra 1998) or PAHs (Joblin et al. 1992, Li & Draine 2001a, Cecchi-Pestellini et al. 2008, Steglich et al. 2010).

The far-UV part ($\lambda \gtrsim 6 \mu\text{m}^{-1}$) of the Galactic interstellar extinction continues to rise up with shorter wavelength to $\lambda = 0.1 \mu\text{m}$ and there does not appear to be any evidence of saturation even at this wavelength.⁴ Since it is generally true that a grain absorbs and scatters light most effectively at wavelengths comparable to its size $\lambda \approx 2\pi a$, we can therefore conclude that there must be appreciable numbers of ultrasmall grains with $a \lesssim 0.1 \mu\text{m}/2\pi \approx 16 \text{ nm}$. In the far-UV wavelength range, the grains of a couple of nanometers are in the Rayleigh regime (i.e. $2\pi a/\lambda \ll 1$) and their extinction cross sections per unit volume, $C_{\text{ext}}(a, \lambda)/V$, are independent of size. Hence the far-UV extinction indicates the presence of nanodust, but does not allow to constrain the sizes of the nanodust in the ISM.

3 Emission Brightness from Nanodust and Molecules

While the far-UV interstellar extinction requires the presence of a population of nano-sized grains in the ISM, the near- and mid-IR⁵ emissions provide constraints of their size and composition. The nanodust is seen by its stochastic heating and by its characteristic emission.

A dust particle in space is subject to substantial temporal fluctuations in temperature, if (i) its heat content is smaller than or comparable to the energy of a single stellar photon (Greenberg 1968), and (ii) the photon absorption rate is smaller than the radiative cooling rate (Li 2004). In the diffuse ISM, nanodust is stochastically heated by single photons to temperatures much higher than its “equilibrium” temperature (even though an “equilibrium” temperature is not physical for a stochastically-heated nanograin, it can still be *mathematically* determined from the energy balance between absorption and emission).

Figure 2 illustrates the time evolution of grain temperature within a day for four PAH/graphitic grains exposed to the solar neighbourhood interstellar radiation field (Draine 2003). We see that for grain radii $a \gtrsim 20 \text{ nm}$, individual photon absorptions are relatively frequent, and the grain heat capacity is large enough that the temperature excursions following individual photon absorptions are relatively small; it is reasonable to approximate the grain temperature as being constant in time. Grains with radii, $a \lesssim 5 \text{ nm}$, however, cool appreciably in the time between photon absorptions; as a result, individual photon absorption events raise the grain temperature to well above the mean value. A PAH molecule of 100 carbon atoms (corresponding to a size of $\sim 6 \text{ \AA}$)⁶ will even be heated to $T \approx 785 \text{ K}$ by a photon of $h\nu = 6 \text{ eV}$, while its

⁴ However, the Kramers-Kronig dispersion relation requires that the far-UV extinction rise with inverse wavelengths must turn over at some smaller wavelengths as the wavelength-integrated extinction must be a finite number (see Purcell 1969).

⁵ We here use “near-IR” for wavelengths $1 \mu\text{m} \lesssim \lambda \lesssim 12 \mu\text{m}$, “mid-IR” for $12 \mu\text{m} \lesssim \lambda \lesssim 60 \mu\text{m}$, and “far-IR” for $60 \mu\text{m} \lesssim \lambda \lesssim 1000 \mu\text{m}$.

⁶ The term “PAH size” refers to the radius a of a spherical grain with the same carbon density as graphite (2.24 g cm^{-3}) and containing the same number of carbon atoms N_C : $a \equiv 1.286 N_C^{1/3} \text{ \AA}$.

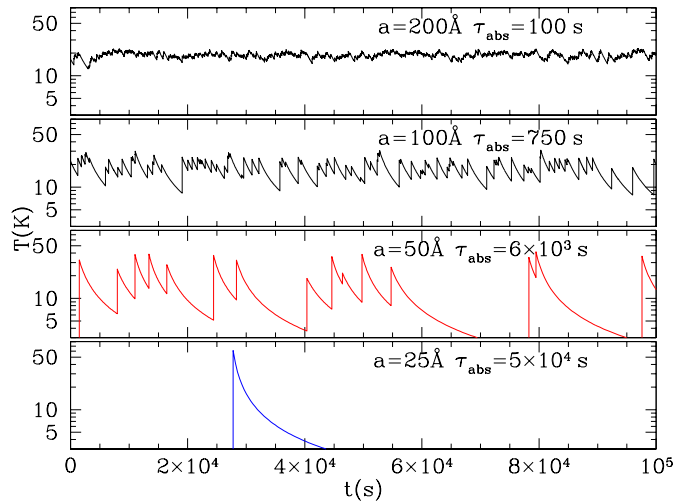


Fig. 2. The time evolution of grain temperature within a day ($\sim 8.6 \times 10^4$ s) for four PAH/graphitic grains exposed to the solar neighbourhood interstellar radiation field. τ_{abs} is the mean time between photon absorptions. Grains with radii $a \gtrsim 20$ nm obtain an equilibrium temperature (i.e. their temperature does not fluctuate much with time) due to their large photon absorption rates $1/\tau_{\text{abs}}$ (because of their large absorption cross sections) and their large heat capacities (so that a single photon cannot significantly raise their temperature). For grains with radii $a \lesssim 5$ nm their temperature strongly fluctuates with time due to their small heat capacities (so that a single photon can result in an appreciable raise of their temperature) and their small photon absorption rates (so that they could have already cooled down before the absorption of another photon). Taken from Draine (2003).

“equilibrium” temperature would just be ~ 22 K. The stochastic heating is further discussed in the appendix.

Andriessse & de Vries (1976) presented the first IR emission evidence for nanodust in the dust cloud in M 17, a star-forming nebula. They found that the $8\text{--}20 \mu\text{m}$ emission spectrum is similar over a distance of $\sim 2'$ through the source, suggesting a constant dust temperature. Since large, submicron-sized grains would attain equilibrium temperatures that decrease with distance from the illuminating source, Andriessse (1978) interpreted this as due to stochastically heated grains of ~ 1 nm.

A more definite piece of observational evidence was provided by Sellgren et al. (1983). In near-IR observations of three visual reflection nebulae (i.e. NGC 7023, 2023, and 2068), they discovered that each nebula has extended near-IR emission consisting of emission features at 3.3 and $3.4 \mu\text{m}$ and a smooth continuum characterized by a color temperature ~ 1000 K. Both the $3.3 \mu\text{m}$ feature and the color temperature of the continuum show very little variation from source to source and within a given source with distance from the central star. Sellgren (1984) argued that this emission could not be explained by thermal emission from dust in radiative equilibrium with the central star since otherwise the color temperature of this emission should fall off rapidly with distance from the illuminating star; instead, she proposed that this emission is due to stochastically heated nanodust.

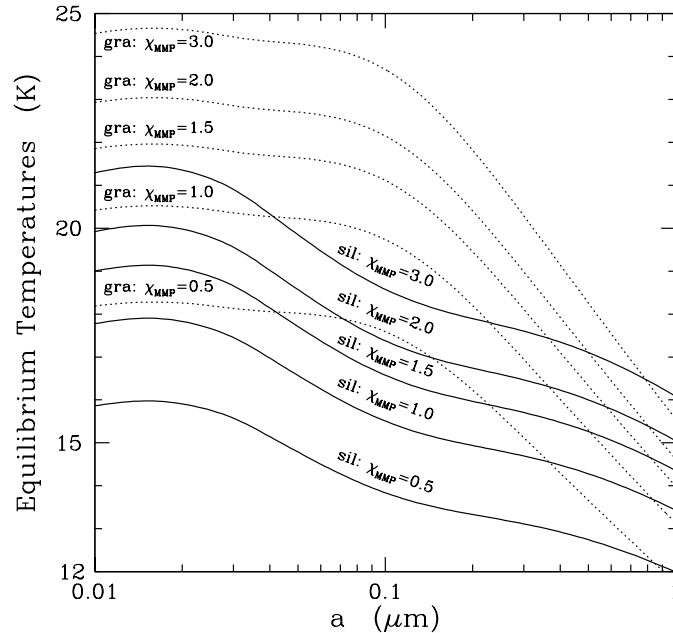


Fig. 3. Equilibrium temperatures for graphite (dotted lines) and silicate grains (solid lines) in environments with various starlight intensities (χ_{MMP} , in units of the Mathis, Mezger, & Panagia (1983) solar neighbourhood interstellar radiation field). Both silicate and graphitic grains larger than 10–20 nm attain equilibrium temperatures in the range of $12\text{ K} < T < 25\text{ K}$ and these grains are too cold to emit appreciably at $\lambda < 60\ \mu\text{m}$. The equilibrium temperatures of grains with $a < 20\text{ nm}$ do not depend on their size. Taken from Li & Draine (2001a).

Infrared observations from satellites are made since the 1980s and today the ISM is known for a broad spectral interval (Figure 4). Initially the diffuse ISM emission observed at $12\ \mu\text{m}$ and $25\ \mu\text{m}$ suggested the presence of nanodust, since it exceeds the emission from large grains with $\sim 12\text{--}25\text{ K}$ thermal equilibrium temperature (Fig. 3) by several orders of magnitude (Boulanger & Perault 1988). Later observations showed broadband emission at $3.5\ \mu\text{m}$ and $4.9\ \mu\text{m}$ (Arendt et al. 1998), as well as at $3.3, 6.2, 7.7, 8.6,$ and $11.3\ \mu\text{m}$ (Onaka et al. 1996, Tanaka et al. 1996, Mattila et al. 1996). These emission features are collectively referred to as the “UIR” bands, and often attributed to PAH molecules (Léger & Puget 1984, Allamandola et al. 1985).

We now discuss a particular model to explain the different ISM dust observations. Figure 5 shows a comparison of the observed emission with the emission calculated from the silicate-graphite-PAH model (Li & Draine 2001a). In this model, $\sim 15\%$ of the carbon is locked up in the PAH component and the near-IR and UIR spectrum are best reproduced by PAHs with a log-normal size distribution peaking at $a \sim 6\ \text{\AA}$, corresponding to ~ 100 carbon atoms. At $\lambda \lesssim 60\ \mu\text{m}$ the emission is predominantly from small carbonaceous grains (graphite and PAHs) with $a < 25\text{ nm}$. Even at $\lambda = 60\ \mu\text{m}$, the grains with $a < 25\text{ nm}$ contribute $\sim 70\%$ of the total emission power of the diffuse ISM. The large silicate and graphite grains of $a > 25\text{ nm}$ together

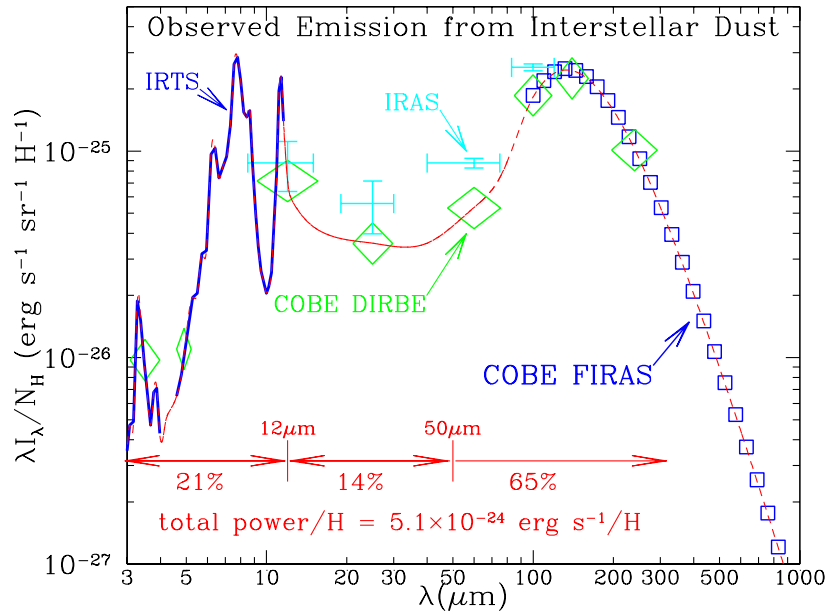


Fig. 4. Observed diffused emission of interstellar dust from the *Infrared Astronomical Satellite* (IRAS), the *Infrared Telescope in Space* (IRTS), the *Spitzer Space Telescope* (Spitzer), and the *Cosmic Background Explorer* (COBE) satellite with its *Far Infrared Absolute Spectrophotometer* (FIRAS) and its *Diffuse Infrared Background Experiment* (DIRBE). The total IR emission normalized to the hydrogen column density N_{H} , is $\sim 5.1 \times 10^{-24} \text{ erg s}^{-1} \text{ H}^{-1}$. The crosses denote observations from IRAS (Boulanger & Perault 1988), squares from COBE-FIRAS (Finkbeiner et al. 1999), diamonds from COBE-DIRBE (Arendt et al. 1998), and the heavy curve from IRTS (Onaka et al. 1996, Tanaka et al. 1996). The “UIR” bands at $3.3\text{--}11.3 \mu\text{m}$ (generally attributed to PAHs) account for $\sim 20\%$ of the total IR emission, the emission from nanodust at $\lambda \lesssim 60 \mu\text{m}$ accounts for $\gtrsim 35\%$ and the submicron-sized grain population emits mostly at $\lambda \gtrsim 60 \mu\text{m}$ and accounts for $\lesssim 65\%$. Taken from Draine (2003).

dominate the emission at $\lambda > 60 \mu\text{m}$, accounting for $\sim 35\%$ of the total IR power. The far-IR emission at $\lambda > 100 \mu\text{m}$ can be closely approximated by a modified black body of $I_{\lambda} \propto \lambda^{-\beta} B_{\lambda}(T)$ with $\beta \approx 1.7$ and $T \approx 19.5 \text{ K}$ (see Draine 1999) or by model emission calculated from large grains with $a > 25 \text{ nm}$. The emission at $\lambda = 12, 25 \mu\text{m}$ and shorter wavelengths (as well as part of the $60 \mu\text{m}$ band) cannot be explained by large grains and it requests a population of stochastically heated nanodust.

4 Microwave Emission from Rotationally-Excited Nanodust

Numerous sensitive experiments to map the microwave sky have revealed unexpected emission at 10–100 GHz frequencies (see Figure 6). The spectral variation and absolute value of this “anomalous” component of the diffuse foreground microwave

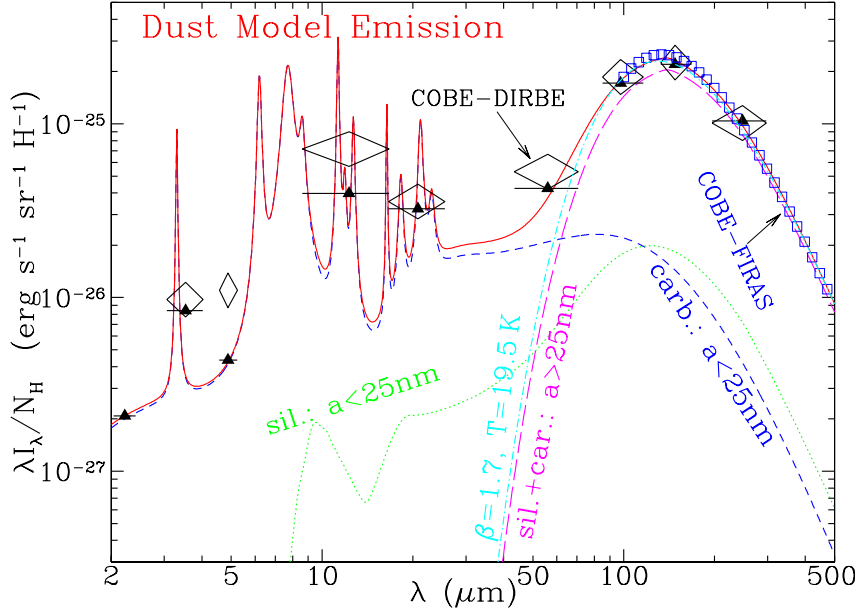


Fig. 5. Comparison of the ISM dust model to the observed emission from the diffuse ISM. Dotted green line: small silicate grains with $a < 25$ nm; Dashed blue line: small carbonaceous grains (graphite and PAHs) with $a < 25$ nm; Long dashed magenta line: the sum of big silicate and graphite grains with $a > 25$ nm; Dot-dashed cyan line: a modified gray body of $I_\lambda \propto \lambda^{-\beta} B_\lambda(T)$ with $\beta \approx 1.7$ and $T \approx 19.5$ K approximating the far-IR emission at $\lambda > 100 \mu\text{m}$ determined by DIRBE-FIRAS. Triangles show the model spectrum (solid curve) convolved with the DIRBE filters. Observational data are from DIRBE (diamonds; Arendt et al. 1998), and FIRAS (squares; Finkbeiner et al. 1999). For abbreviations see caption to Fig. 4. Taken from Li & Draine (2001a).

emission are very different from those of the traditional diffuse emissions at these frequency ranges (e.g. the free-free, synchrotron, and thermal dust emission have power-law-like spectra at microwave frequencies) and can not easily be explained with them.

The spatial distribution of this microwave emission is correlated with interstellar dust emission at $100 \mu\text{m}$ and $140 \mu\text{m}$ (see Draine 2003), and even better correlated with the mid-IR emission (Casassus et al. 2006, Ysard et al. 2010, Vidal et al. 2011).

This suggests its origins from the dust, but extrapolating the 100–3000 μm far-IR emission of large dust ($a > 25$ nm) to the microwave frequencies provides values far below the observed microwave emission (see Figure 6). For these reasons, the electric dipole radiation from rapidly spinning nanograins has become the best explanation for the “anomalous” microwave emission.

A spinning grain with an electric dipole moment μ radiates power $P = 2\omega^4 \mu^2 \sin^2 \theta / 3c^3$, where θ is the angle between the angular velocity ω and μ , and c is the speed of light. The angular velocity $\omega = J/I$, where J is the grain angular momentum, and I

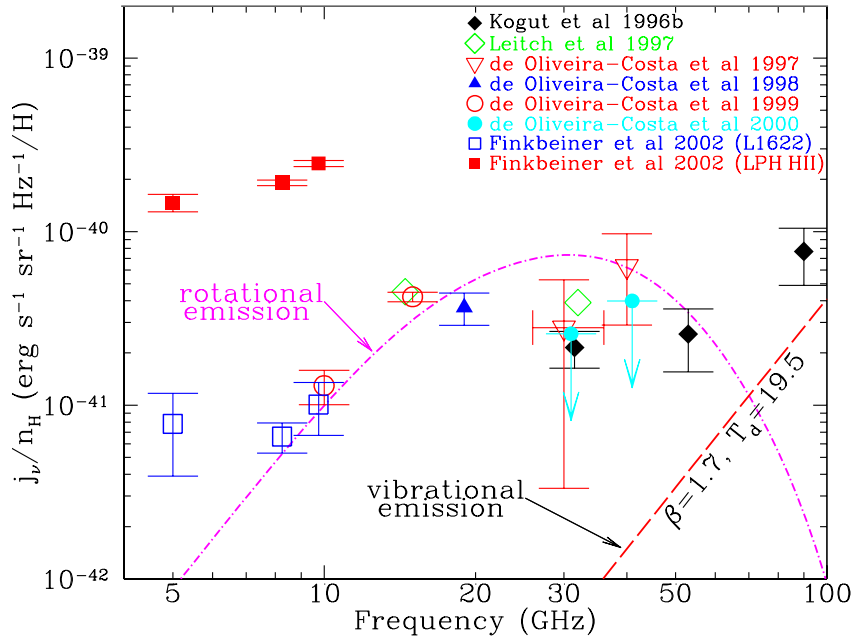


Fig. 6. Comparison of the “anomalous” Galactic foreground microwave emission in the 10–100 GHz frequency region with the rotational electric dipole emission calculated from fast-spinning nanograins (i.e. PAHs) which account for the “UIR” vibrational emission (see Figures 4, 5). Symbols: observational determinations of “anomalous microwave emission”. Dot-dashed line: model rotational emission spectrum of nanodust (Draine & Lazarian 1998). Dashed line: low-frequency tail of the emission from large grains (mostly with $a > 25$ nm) (also see Figures 4, 5). Taken from Draine (2003).

is the moment of inertia of the grain. For spherical grains, $I \propto a^5$. Hence angular velocity steeply decreases with grain size and in interstellar environments only nanograins can be driven to rotate fast enough to emit at microwave frequencies. For a PAH grain of radius $a = 1$ nm in the diffuse ISM, J peaks at $\sim 2000 \hbar$ (see Draine & Lazarian 1998).

As described by Draine and his coworkers (Draine & Lazarian 1998, Hoang et al. 2010), a number of physical processes, including collisions with neutral atoms and ions, “plasma drag” (due to interaction of the electric dipole moment of the grain with the electric field produced by passing ions), and absorption and emission of photons, can drive nanograins to rapidly rotate, with rotation rates reaching tens of GHz. The rotational electric dipole emission from these spinning nanograins, the very same grain component (i.e. PAHs) required to account for the “UIR” emission and the observed 12 and 25 μm continuum emission, was shown to be capable of accounting for the “anomalous” microwave emission (Draine & Lazarian 1998; see Figure 6). Vidal et al. (2011) found that the microwave emission at 31 GHz of the LDN 1780 translucent cloud correlates better with the 12, 25 μm emission than with

the $100\ \mu\text{m}$ emission, which supports that emission at this frequency originates from nanodust.

We should note that although the electric dipole radiation from spinning nanodust provides the best explanation for the “anomalous” microwave emission, other physical mechanisms (e.g. hot free-free emission, hard synchrotron radiation, or magnetic dipole emission) could still be contributing at some level (e.g. see Draine & Lazarian 1999).

5 Extended Red Emission: Photoluminescence from Nanodust

Dust *emission* at optical wavelengths, not expected from its vibrational excitation, is also seen in the red part of the visible spectra of a wide variety of dusty environments (which cannot be accounted for just by dust scattering alone). This emission is termed “extended red emission” (ERE). It is characterized by a broad, featureless band between $\sim 5400\ \text{\AA}$ and $9500\ \text{\AA}$, with a width of $600\ \text{\AA} \lesssim \text{FWHM} \lesssim 1000\ \text{\AA}$ and a peak of maximum emission at $6100\ \text{\AA} \lesssim \lambda_p \lesssim 8200\ \text{\AA}$, depending on the physical conditions of the environment where the ERE is produced (see Figure 7). The peak wavelength λ_p varies from source to source and within a given source with distance from the illuminating star. The ERE width appears to increase as λ_p shifts to longer wavelengths (Darbon et al. 1999). This suggests that the ERE carriers can be easily modified (or destroyed) by intense UV radiation, as λ_p is related to the size of the carrier grain.

The ERE has been seen in various astrophysical regions: the diffuse ISM of our Galaxy and other galaxies, reflection nebulae, planetary nebulae, and HII regions, which, in terms of UV photon densities, span a range of six orders of magnitudes, and in terms of dust, represent both heavily processed interstellar dust and relatively “fresh” dust produced in local outflows (e.g. planetary nebulae and the proto-planetary nebula Red Rectangle; see Witt & Vijh 2004).

The ERE is commonly attributed to photoluminescence (PL) by some component of interstellar dust, a process in which absorptions of UV photons are followed by electronic transitions associated with the emission of optical or near-IR photons. The ERE is powered by UV/visible photons, as demonstrated by Smith & Witt (2002) who found that the maximum ERE intensity in any given environment is closely correlated with the density of UV photons.

The true nature of the ERE carriers still remains unknown, although over a dozen candidates have been proposed over the past decades. For a proposed candidate to be valid, it must luminesce in the visible with its spectrum matching that of the observed ERE. But this is not sufficient. As many candidate materials luminesce in the visible after excitation by UV photons, along with the carrier abundance, the efficiency for photoluminescence – the quantum efficiency for the conversion of UV photons absorbed by the ERE carrier to ERE photons – represents one of the strongest constraints.

Gordon et al. (1998) placed a lower limit on the photon conversion efficiency η_{PL} (measured by the number ratio of luminesced photons to exciting UV photons) to be approximately $(10 \pm 3)\%$ (also see Szomoru & Guhathakurta 1998). This lower limit was derived from the correlation of ERE intensity with HI column density at high Galactic latitudes (Gordon et al. 1998), with the assumption that *all UV absorption is due to the ERE carrier candidate* (in other words, assuming that *all*

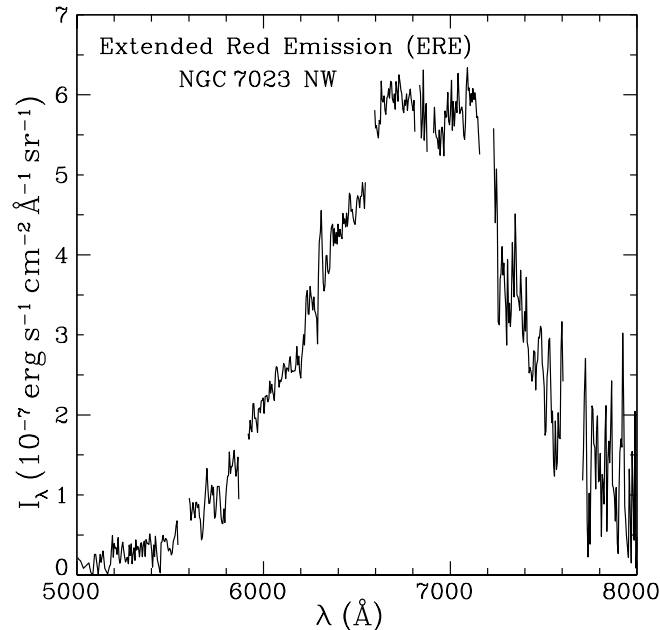


Fig. 7. Observed photoluminescence spectrum – the “Extended Red Emission” (ERE) arising from an unidentified nanodust species in the north-west (NW) filament of NGC 7023, a reflection nebula. Data taken from Witt & Vijh (2004).

the UV photons absorbed by dust lead to the production of ERE). As there are other known absorbing interstellar dust components not likely associated with ERE, the actual luminescing efficiency must be substantially larger than 10%, perhaps in the vicinity of 50% or even higher (Smith & Witt 2002). This poses a serious challenge to materials once thought to be promising ERE candidates, as their luminescing efficiencies are $< 1\%$ (see Wada et al. 2009, Godard & Dartois 2010).

All these suggest that the ERE carriers are very likely in the nanometer size range because (a) in general, nanograins are expected to luminesce efficiently through the recombination of the electron-hole pair created upon absorption of an energetic photon, since in such small systems the excited electron is spatially confined and the radiationless transitions that are facilitated by Auger- and defect-related recombination are reduced; and (b) small nanograins may be photolytically more unstable and/or more readily photoionized in regions where the radiation intensity exceeds certain levels of intensity and hardness, and thus resulting in both a decrease in the ERE intensity and a redshift of the ERE peak wavelength.⁷ Observationally, Darbon

⁷ This is because (i) photoionization would quench the luminescence of nanograins, and (ii) the smaller grains would be selectively removed due to size-dependent photofragmentation (Smith & Witt 2002). Due to the quantum confinement effect, the band gap of a semiconductor-like nanograin is *smaller* (and therefore the wavelength of luminescing photons is *longer*) for a *bigger* nanograin (see §4 in Li 2004).

et al. (1999) and Smith & Witt (2002) showed that the ERE peak wavelength is indeed shifted toward longer wavelengths with increasing UV radiation density.

Several materials have been proposed as ERE carriers: carbon nanoparticles (Seahra & Duley 1999), silicon nanoparticles (Witt et al. 1998, Ledoux et al. 1998; but see Li & Draine 2002), nanodiamonds (Chang et al. 2006), and PAH clusters (Berne et al. 2008). But none of them satisfies all the observational requirements (see Li 2004).

6 Photoelectric Heating of the ISM Gas by Nanodust

In the Milky Way galaxy, approximately 60% (by mass) of the gas is in atomic hydrogen (HI) regions. Observations of the 21 cm line,⁸ show that the diffuse neutral atomic gas in the ISM is in two distinct phases with temperatures ~ 100 K (“Cold Neutral Medium”, which accounts for, by mass, $\sim 40\%$ of the HI in HI regions) and ~ 6000 K (“Warm Neutral Medium”, which accounts for $\sim 60\%$ of the HI in HI regions). What heats the HI gas to temperatures of ~ 100 K or ~ 6000 K? One possible answer to this question provides indirect evidence for the existence of an appreciable quantity of nanodust in the ISM.

It has long been recognized that interstellar grains are an important energy source for heating the interstellar gas through ejection of photoelectrons because (a) photons with energies below the ionization potential of H (~ 13.6 eV) do not couple directly to the gas; and (b) other heating sources such as cosmic rays, magnetic fields, and turbulence are not important as a global heating source for the diffuse ISM (e.g. the cosmic ray flux is too low by a factor of ~ 10 to account for the interstellar gas heating; Watson 1972).

The photoelectric heating starts from the absorption of a UV photon by a dust grain, followed by ejection of an electron (“photoemission”). The photoelectron diffuses toward the grain surface and transfers (through inelastic collision) to the gas the excess (kinetic) energy left over after overcoming the work function (the binding energy of the electron to the grain) and the electrostatic potential (i.e. Coulomb attraction) of the grain (if it is charged).

In the diffuse ISM, nanodust (and in particular, angstrom-sized PAH molecules) are much more efficient in heating the gas than large grains (see Tielens 2008) since (a) the mean free path of an electron in a solid is just ~ 1 nm and therefore photoelectrons created inside a large grain rarely reach the grain surface; and (b) the total far-UV absorption is dominated by the nanodust component (see §3). Theoretical studies have shown that grains smaller than 10 nm are responsible for $\gtrsim 96\%$ of the total photoelectric heating of the gas, with half of this provided by grains smaller than 1.5 nm (Bakes & Tielens 1994, Weingartner & Draine 2001b). Figure 8 shows the calculated photoelectric heating rate as a function of grain size, illustrating that the photoelectric heating is dominated by the smallest grains (i.e. PAHs) present in the ISM.⁹

⁸ The 21 cm line originates in the hyperfine splitting of the parallel and antiparallel spin states of the electron (relative to the spin of the proton) in the electronic ground state ($1s$) of atomic H.

⁹ In the diffuse ISM, PAHs and PAH clusters (or very small graphitic grains) dominate the nanodust population. Nondetection of the $9.7 \mu\text{m}$ silicate Si–O emission

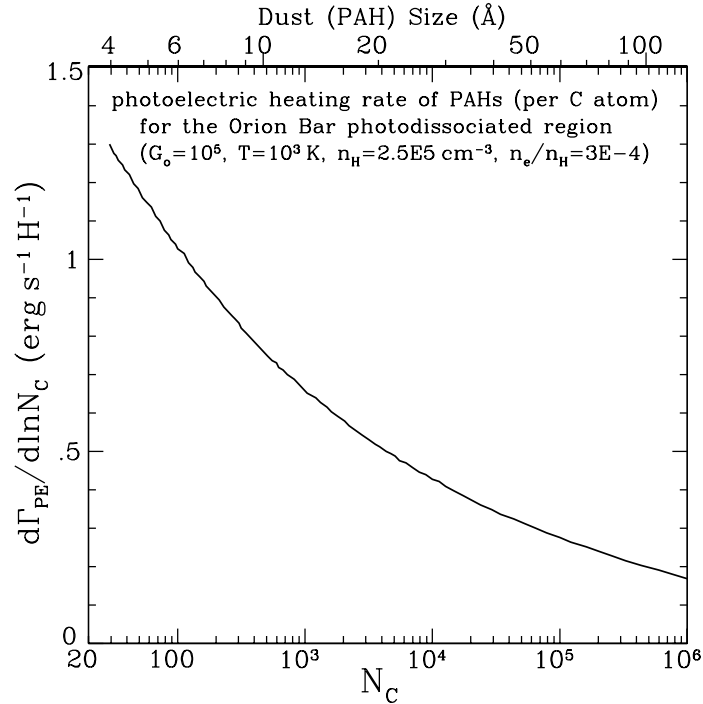


Fig. 8. The photoelectric heating rate Γ_{PE} of the interstellar gas in the Orion Bar photodissociated region as a function of PAH size (measured by N_{C} , the number of carbon atoms; the upper axis label gives the graphite-equivalent spherical radius $a \approx 1.286 N_{\text{C}}^{1/3} \text{ \AA}$, or $N_{\text{C}} \approx 0.468 (a/\text{\AA})^3$). The rates are presented in such a way that equal areas under the curve correspond to equal contributions to the heating. Typically, approximately half of the heating originates from PAHs and PAH clusters (with $N_{\text{C}} < 10^3$ or $a < 1.3 \text{ nm}$). The other half is contributed by grains of sizes $1.3 \text{ nm} < a < 10 \text{ nm}$). Larger grains do not contribute noticeably to the heating. Data taken from Bakes & Tielens (1994).

Observations confirm the dominant role of nanodust in the gas heating through the photoelectric effect. For instance, Habart et al. (2001) studied the major cooling lines, [CII] $158 \mu\text{m}$ and [OI] $63 \mu\text{m}$, of L 1721, an isolated cloud illuminated by a B2 star in the ρ Ophiuchi molecular complex. Because of the energy balance between heating and cooling, the [CII] $158 \mu\text{m}$ and [OI] $63 \mu\text{m}$ cooling lines (which dominate the gas cooling) reflect the heating input to the gas. They found that the spatial distribution of the gas cooling lines closely correlate with that of the mid-IR emission attributed to nanodust (and PAHs).

feature in the diffuse ISM (see Figure 4) indicates that nano silicate grains are not abundant (see Li & Draine 2001b).

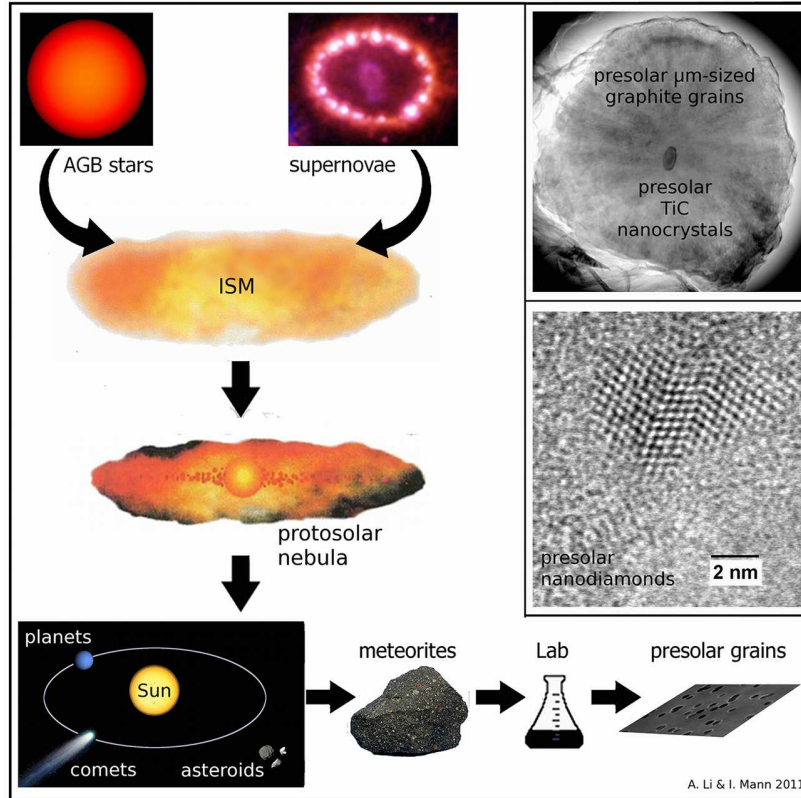


Fig. 9. A schematic illustration of the history of presolar grains from their condensation in stellar winds of AGB (*Asymptotic Giant Branch*) stars or in supernova ejecta, to their injection into the ISM, and subsequent incorporation into the dense molecular cloud from which our solar system formed (i.e. protosolar nebula). These grains survived all the violent processes occurring in the ISM (e.g. sputtering by shock waves) and in the early stages of solar system formation and were incorporated into meteorite parent bodies. Experimental studies in terrestrial laboratories allow to separate them from the meteorite or interplanetary dust material in which they are embedded. Inserted are the TEM (*Transmission Electron Microscopy*) images of presolar nanodiamond grains (Banhart et al. 1998) and a presolar TiC nanocrystal within a micrometer-sized presolar graphite spherule (Bernatowicz et al. 1991).

7 Direct Evidence: Presolar Nanodust in Primitive Meteorites

Based on their isotopic anomalies, presolar grains (such as graphite, silicate, silicon carbide SiC, silicon nitride Si₃N₄, and refractory oxides including corundum Al₂O₃, spinel MgAl₂O₄) that predate the solar system have been identified in primitive meteorites, a class of meteorites that essentially remain chemically unaltered since their formation in the solar nebula (e.g. see Lodders 2005). Presolar nanodiamonds

of radii $a \sim 1$ nm (see Figure 9) were found to be rich in primitive carbonaceous meteorites, with an abundance as much as $\sim 0.1\%$ of the total mass in some primitive meteorites, more abundant than any other presolar grains by over two orders of magnitude (Lewis et al. 1987).¹⁰ Presolar titanium carbide (TiC) nanocrystals were also seen in primitive meteorites (see Figure 9). With a mean radius of ~ 3.5 nm, they occur as nano-sized inclusions within micrometer-sized presolar graphitic spherules (Bernatowicz et al. 1991).

These presolar nanograins, after their condensation in stellar outflows from carbon-rich evolved stars (e.g. TiC nano crystals) or in ejecta from supernova explosion (e.g. nanodiamonds), and prior to their incorporation into the parent bodies of meteorites during the early stages of solar system formation, they must have had a sojourn in the ISM out of which the solar system formed (see Figure 9 for illustration).

However, neither nanodiamonds nor TiC nanocrystals could be representative of the bulk composition of interstellar nanograins and one observation is often explained in several different ways (Draine 2003).

8 Summary and Comparison to Nanodust in the Solar System

Based on the discussions in the previous sections we can summarize the observational evidence for the presence of nanodust in the ISM: (i) the far-UV extinction at $\lambda^{-1} > 6 \mu\text{m}^{-1}$ caused by the absorption of nanodust (§2), (ii) the $\sim 2\text{--}60 \mu\text{m}$ near- and mid-IR spectral and continuum emission from stochastically heated nanograins through vibrational relaxation (§3), (iii) the $\sim 10\text{--}100$ GHz “anomalous” Galactic foreground microwave emission from rotationally excited nanograins through electric dipole radiation (§4), and (iv) the $\sim 5400\text{--}9500 \text{ \AA}$ broad, featureless ERE band from electronically excited nanograins through photoluminescence (§5). The presence of an appreciable amount of nanograins in the ISM is also indirectly inferred from the photoelectric heating of interstellar gas by nanodust (i.e. PAHs; §6) and finally presolar grains are found in interplanetary dust and meteorites of the solar system.

Finally, it is worth noting that the nanodust population (particularly PAHs) may be responsible for the lower gas-phase deuterium abundance of $\text{D}/\text{H} \approx 7\text{--}22$ ppm in the Galactic ISM compared to the primordial value of $\text{D}/\text{H} \approx 26$ ppm, through depleting the “missing” D onto PAHs (Draine 2006).

Based on the preceding discussion the physical processes that allow for (direct or indirect) observation of nanodust are UV light-scattering, stochastic heating, electric dipole radiation of rotating nanodust, photoluminescence, and finally photoelectric heating of the surrounding gas.

¹⁰ It is worth noting that, as mentioned earlier, presolar grains are usually recognized by the isotope ratios that are different from those for grains formed in the solar system, but for small nanodiamonds, this method does not work as accurately as for large grains (since they are too small). There are debates that a fraction of the meteoritic nanodiamonds may actually have formed in the early solar system (e.g. see Ott 2007).

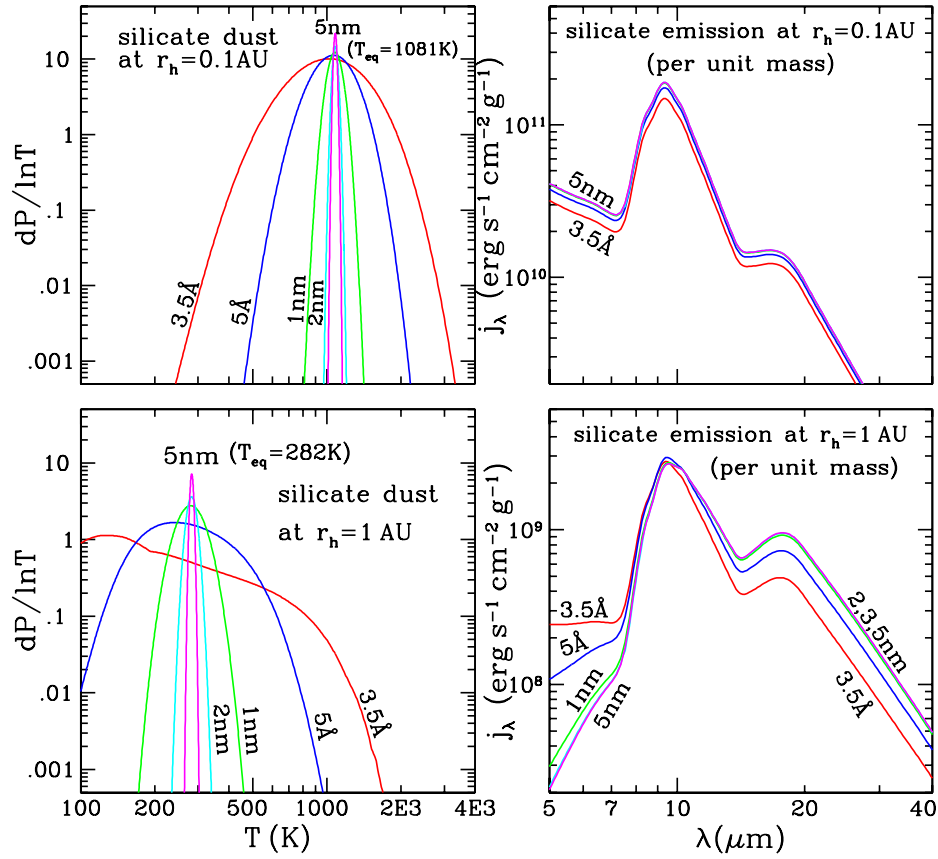


Fig. 10. Temperature probability distribution $dP/d\ln T$ and emission for selected silicate grains heated by the Sun at heliocentric distances of $r_h=0.1, 1\text{AU}$. The $dP/d\ln T$ distribution functions at $r_h=1\text{AU}$ are much broader than that for the same dust at $r_h=0.1\text{AU}$. The grains with $a > 1\text{nm}$ peak at the same temperature (which is their equilibrium temperature), as expected from their Rayleigh scattering nature (see §8).

We now discuss the possible occurrence of these processes in the solar system. It is worth noting at the beginning, that the nanodust in the solar system is not identical to the nanodust in the ISM. The grains with $a < 5\text{nm}$ in the local interstellar cloud in the vicinity of the Sun do not enter the solar system, as they are deflected by the magnetic field that builds up in the outer solar system due to interaction of the local ionized ISM gas with the solar wind (Mann 2010). The nanodust in the solar system is produced locally from the interplanetary dust cloud or from solar system objects.

- **Light-scattering in far UV:** Scattering from interplanetary dust particles generated the Zodiacal light, which is the predominant diffuse brightness to wavelengths as short as $\lambda \sim 0.3 \mu\text{m}$. The brightness at shorter wavelength is dominated by the emission of unresolved stars (45). Dust emission in the X-ray was discussed after the ROSAT survey established comets as a class of X-ray sources. The discussed dust-related X-ray signals are X-ray fluorescence and scattering by nano dust and X-ray emission caused by high-velocity impacts of nano dust. The X-ray flux from nanodust in the solar system is estimated by Kharchenko and Lewkow in this book.
- **Stochastic heating:** For the nanograins in the inner solar system (Mann 2007), it is more likely for them to attain an equilibrium temperature (compared to the same dust in the diffuse ISM). This is because the solar system nanodust is exposed to a far more intense radiation field: at a heliocentric distance of r_h , the $912 \text{ \AA} - 1 \mu\text{m}$ solar radiation intensity is $\approx 7.6 \times 10^7 (r_h/\text{AU})^{-2}$ times that of the local interstellar radiation field, where r_h is the heliocentric distance of the dust from the Sun.

In Figure 10 we present the temperature probability distribution functions of amorphous silicate dust using the dielectric functions of Draine & Lee (1984) for selected sizes ($a = 3.5 \text{ \AA}$, 5 \AA , 1 nm , 2 nm , 5 nm) illuminated by the Sun at $r_h = 0.1, 1 \text{ AU}$. To facilitate comparison, we plot $dP/d \ln T$ in the same T and $dP/d \ln T$ ranges for $r_h = 0.1 \text{ AU}$ and $r_h = 1 \text{ AU}$. The emission is also illustrated in the same λ and j_λ ranges (except the latter differs by a factor of r_h^{-2}). We see that silicate dust with $a \gtrsim 2 \text{ nm}$ attains an equilibrium temperature of $T_{\text{eq}} \approx 282 \text{ K}$ at $r_h = 1 \text{ AU}$. At $r_h = 0.1 \text{ AU}$, the $dP/d \ln T$ distribution functions for grains as small as $a = 1 \text{ nm}$ is already like a delta function, peaking at $T_{\text{eq}} \approx 1081 \text{ K}$. At $r_h = 1 \text{ AU}$, the silicate emission spectra for $a = 2, 3, 5 \text{ nm}$ are almost identical. This is because in the entire UV to far-IR wavelength range, these nanograins are in the Rayleigh regime and their Q_{abs}/a values are independent of size, therefore they obtain an almost identical equilibrium temperature. At $r_h = 0.1 \text{ AU}$, this even applies to smaller grains (e.g. $a = 1 \text{ nm}$). To summarize, in the solar system at $r_h < 1 \text{ AU}$, the stochastic heating effect is small for dust larger than $\sim 1 \text{ nm}$ in radius; for dust smaller than $\sim 5 \text{ \AA}$, it may not survive since the stochastic heating would lead to temperatures exceeding $\sim 2000 \text{ K}$. This is roughly the sublimation temperature of silicate dust, though we point out that the nanodust can have lower sublimation temperature than the bulk material (see Kimura, this book).

- **Electric dipole radiation of rotating dust:** We are not aware of any studies of the rotational dynamics of nanodust in the solar system. We do not expect to see strong microwave emission from the dust in the solar system. Although the ions in the solar system may deliver more angular momentum to a grain than in the diffuse ISM (because of their large abundance and large kinetic energy), the dust will not be driven to rotate as fast as in the diffuse ISM, due to (1) the large grain size of the solar system nanodust population, (2) the strong rotational damping caused by photon emission in the solar system, and (3) the small number densities of nanodust in the directions facing away from the Sun (see other chapters of this book). The nanodust in the solar system seems to be in the nm size range (see other chapters of this book), while the microwave

emission in the ISM arises predominantly from angstrom-sized PAHs. Note that the angular velocity $\omega \propto 1/I$, while $I \propto a^5$.

- **Photoluminescence:** As far as observations in the solar system are concerned a coronal emission that appeared similar to the ERE was speculated to result from silicon nano crystals near the sun (Habbal et al. 2003), but this was challenged on the basis of the dust composition and emission properties (Mann & Murad 2005). As opposed to the ISM the nanodust in the solar system most likely is heterogeneous in composition and covers a broad size interval. This broadens wavelength at which the photoluminescence is observed, which makes its detection near the Sun less likely. At this point we are not aware of an observational result in the optical or IR range confirming the existence of nano dust in the solar system and the detection of nano dust in the interplanetary medium in a similar way like the ERE is unlikely (see Mann & Czechowski 2011 in this book).
- **Photoelectric heating:** For the solar system nanodust, photoelectric heating does not occur because the nanodust is embedded in the high temperature solar wind electrons. Instead, the presence of nanodust in the solar wind would rather lead to cooling, because the solar wind ions charge-exchange and are decelerated when passing a nanograin.

9 Conclusion

Observational data, particularly the near- and mid-IR emission data, allow us to constrain the composition, size distribution and quantity of the nanodust population in the ISM: (i) PAHs and nano-sized graphitic grains are the dominant nanodust species in the ISM; locking up $\sim 15\%$ of the total interstellar carbon, they are responsible for the IR emission at $\lambda < 60 \mu\text{m}$ (including the “UIR” bands) and the microwave emission as well; (ii) nano silicate grains are not important: they *at most* account for $\sim 5\%$ of the total interstellar silicon as indicated by the non-detection of the $9.7 \mu\text{m}$ silicate Si–O emission band in the Galactic diffuse ISM (Li & Draine 2001b). Presolar nanograins (i.e. nanodiamonds and TiC nanocrystals) that are identified in primitive meteorites and interplanetary dust are not an abundant population of the ISM nanodust, but provide the most direct evidence for interstellar nanodust. They were present in the local ISM at the time of the formation of the solar system. The physical processes involving nanodust in the ISM are less important for the nanodust in the solar system. Though considering the stochastic heating process suggests that the size of the silicate nanodust in the inner solar system is constrained to $a \gtrsim 0.5 \text{ nm}$.

Appendix: Interstellar Extinction

For the ISM in the solar neighborhood (i.e. a few kiloparsecs from the Sun and within $\sim 100 \text{ pc}$ of the galactic plane), the mean visual extinction has long been determined quite accurately. The interstellar extinction curve is most commonly derived utilizing the “pair” method. As illustrated in Figure 11, this technique involves photometric or spectrophotometric observations of two stars of identical spectral types, with one star located behind a dust cloud and another star, (in ideal case) unaffected by

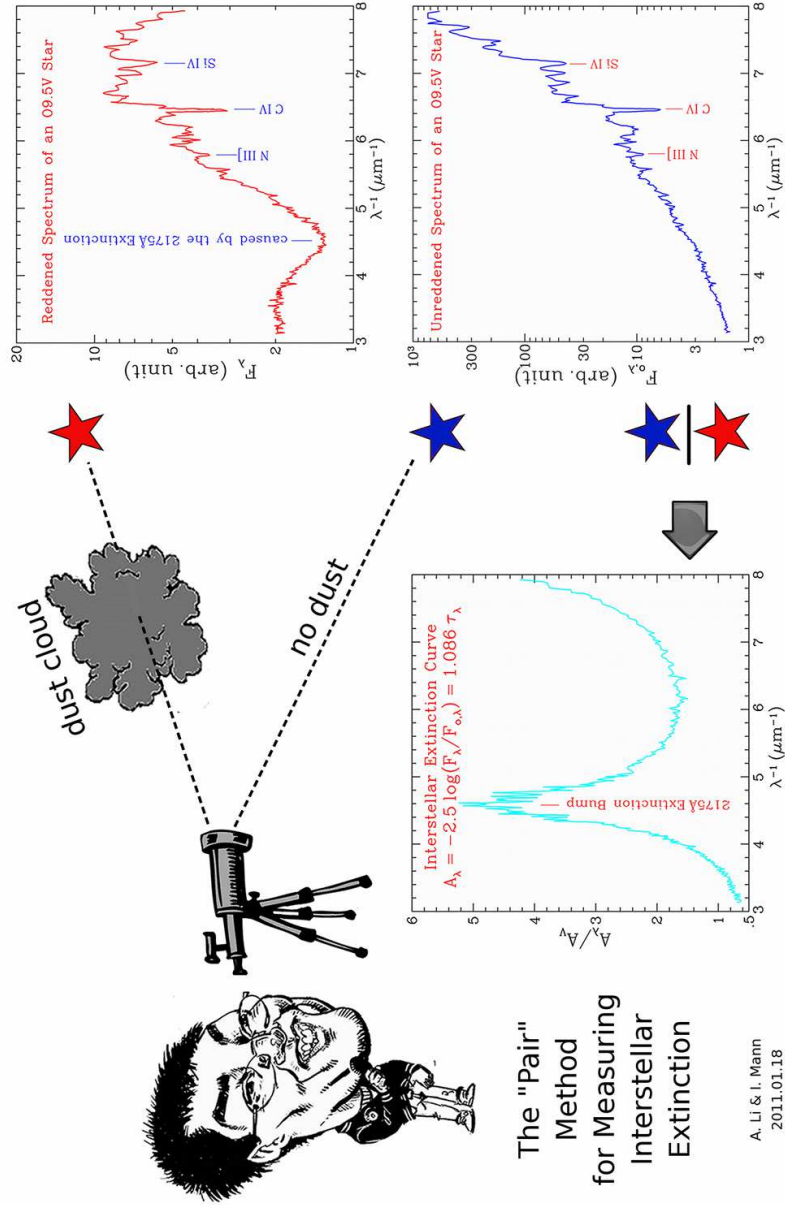


Fig. 11. A conceptual illustration of the "pair" method.

interstellar dust, so that there is no obscuration between the observer and the star. Let F_λ be the observed flux from the reddened star, and $F_{o,\lambda}$ be the flux from the unreddened star. If both stars are located at an identical distance, the extinction A_λ – measured in “magnitudes” – is

$$A_\lambda \equiv 2.5 \log_{10} [F_{o,\lambda}/F_\lambda] \approx 1.086\tau_\lambda \quad (1)$$

where τ_λ is the optical depth. As it is often not possible to find reddened/unreddened star pairs of identical spectral types which are also located at identical distances, one often measures the color excess

$$E(\lambda - V) \equiv A_\lambda - A_V = 2.5 \log_{10} \left[\frac{F_{o,\lambda}/F_{o,V}}{F_\lambda/F_V} \right] \quad (2)$$

from normalized stellar fluxes, with the V band being the usual choice for the normalization purpose. The total-to-selective extinction ratio

$$R_V \equiv A_V/E(B - V) \quad (3)$$

suggested by (Cardelli et al. 1989) is frequently used to characterize the galactic extinction curves.

For particles in the Rayleigh regime (i.e. $2\pi a/\lambda \ll 1$) their extinction cross sections per unit volume, $C_{\text{ext}}(a, \lambda)/V$, are independent of size. Therefore, the observational quantity A_λ/N_{H} ($\text{mag cm}^{-2}\text{H}^{-1}$) – the extinction per unit H column – only constrains $V_{\text{tot}}/n_{\text{H}}$, the total dust volume per H nuclei of this grain component:

$$A_\lambda/N_{\text{H}} = 1.086 \int C_{\text{ext}}(a, \lambda) n_{\text{H}}^{-1} (dn/da) da = 1.086 (V_{\text{tot}}/n_{\text{H}}) (C_{\text{ext}}/V), \quad (4)$$

where dn is the number of grains in the size interval $[a, a + da]$, and N_{H} (n_{H}) is the hydrogen column (volume) density. This explains why the MRN silicate-graphite model with a lower size cut-off of $a_{\text{min}} = 5 \text{ nm}$ (Mathis et al. 1977), that was frequently used before the presence of nanodust was confirmed, could also closely reproduce the observed extinction curve. The MRN model fitted the extinction curve using a mixture of silicate and graphite grains with a simple power-law size distribution: $dn/da \propto a^{-3.5}$ for $5 \text{ nm} \lesssim a \lesssim 0.25 \mu\text{m}$.

The 2175 Å bump is thought to be predominantly due to absorption, as indicated by the broad minimum near 2175 Å of the interstellar albedo (Whittet 2003). The interstellar albedo is defined as the ratio of scattering to extinction. The interstellar extinction is the combination of scattering and absorption. For grains in the Rayleigh limit, the scattering is negligible in comparison with the absorption (see Li 2008). This suggests that its carrier is sufficiently small to be in the Rayleigh limit, with a size $a \ll \lambda/2\pi \approx 35 \text{ nm}$.

Finally, we should note that a smooth extension of the MRN $dn/da \propto a^{-3.5}$ size distribution down to $a = 3 \text{ \AA}$ is not sufficient to account for the observed $12 \mu\text{m}$ and $25 \mu\text{m}$ emission (see Draine & Anderson 1985, Weiland et al. 1986) and that an extra population of nano-sized dust is required (e.g. see Désert et al. 1990, Dwek et al. 1997, Li & Draine 2001a). In the recent Weingartner & Draine (2001a) model, for instance, the grain size distribution extends from a few angstroms to a few micrometers, with $\sim 6\%$ of the total dust mass in grains smaller than 2 nm.

Appendix: Stochastic Heating

Typically large dust particles in the interstellar medium reach equilibrium temperature for which the rate of radiative cooling equals the time-averaged rate of energy absorption. If the emissivity of the dust material is roughly constant with wavelength (which is the case for a sufficiently large dust particle) then the spectral slope of the thermal emission brightness is roughly that of a black body (Planck curve) with the location of maximum emission being determined by the temperature. For interpreting astronomical observations a dust temperature is often assumed to be the equilibrium temperature and one denotes as colour temperature of an object the temperature of a blackbody with peak emission at the same wavelength as the observed brightness. The required dust temperature to generate peak emission in the mid-IR is, for instance ~ 300 K for the $12\ \mu\text{m}$ emission and ~ 150 K for the $25\ \mu\text{m}$ emission. When discussing nanodust, researchers often use the Debye temperature Θ which is a parameter (with a dimension of kelvin) that characterizes the low-temperature heat capacity U of a solid.

Nanograins are small enough that their time-averaged internal energy is smaller than or comparable to the energy of the starlight photons that heat the grains. Stochastic absorption of photons therefore results in transient “temperature spikes”, during which much of the energy deposited by the starlight photon is reradiated in the near- or mid-IR.

The “temperature spike” – the maximum temperature to which a nanograin can reach upon an absorption of a photon is sensitive to its heat capacity (which is $\propto a^3$). When illuminated by a radiation field, the observed intensity I_λ from the transiently heated nanograins is

$$I_\lambda = N_{\text{H}} \int C_{\text{abs}}(a, \lambda) n_{\text{H}}^{-1} (dn/da) da \int B_\lambda(T) (dP/dT)_a dT \quad (5)$$

where $C_{\text{abs}}(a, \lambda)$ is the absorption cross section for a grain of radius a at wavelength λ , $B_\lambda(T)$ is the Planck function at temperature T , and $(dP/dT)_a$ is the dust temperature distribution function which is sensitive to grain size a (see Li 2004). We see that although in the IR wavelength range $C_{\text{abs}}(a, \lambda)/V$ is independent of grain size a , $(dP/dT)_a$ is a sensitive function of a and therefore I_λ allows us to constrain the size distribution of the nanodust component through $(dP/dT)_a$.

Figure 12 shows the temperature probability distributions $dP/d \ln T$ for PAH ions of selected sizes (at $a > 5$ nm their optical properties approach that of graphite; see Li & Draine 2001a). The distributions are shown for $\chi_{\text{MMP}} = 1$ and $\chi_{\text{MMP}} = 10^4$, where χ_{MMP} is the starlight intensity in units of the interstellar radiation field given by Mathis, Mezger, & Panagia (1983) (MMP). We see in Figure 12a that small grains undergo extreme temperature excursions (e.g. the $a = 3.55\ \text{\AA}$ PAH occasionally reaches $T > 2000$ K), whereas larger grains (e.g. $a = 30$ nm) have temperature distribution functions that are very strongly-peaked and like a delta-function, corresponding to only small excursions around an equilibrium temperature. It is apparent that when the rate of photon absorption increases, the “equilibrium” temperature approximation becomes valid for smaller grains; e.g., for $\chi_{\text{MMP}} = 10^4$ one could approximate a $a = 5$ nm grain as having an equilibrium temperature $T_{\text{eq}} \approx 150$ K whereas for $\chi_{\text{MMP}} = 1$ the temperature excursions are very important for this grain (see Draine & Li 2007). This is also the reason for stochastic heating not being important in the inner solar system.

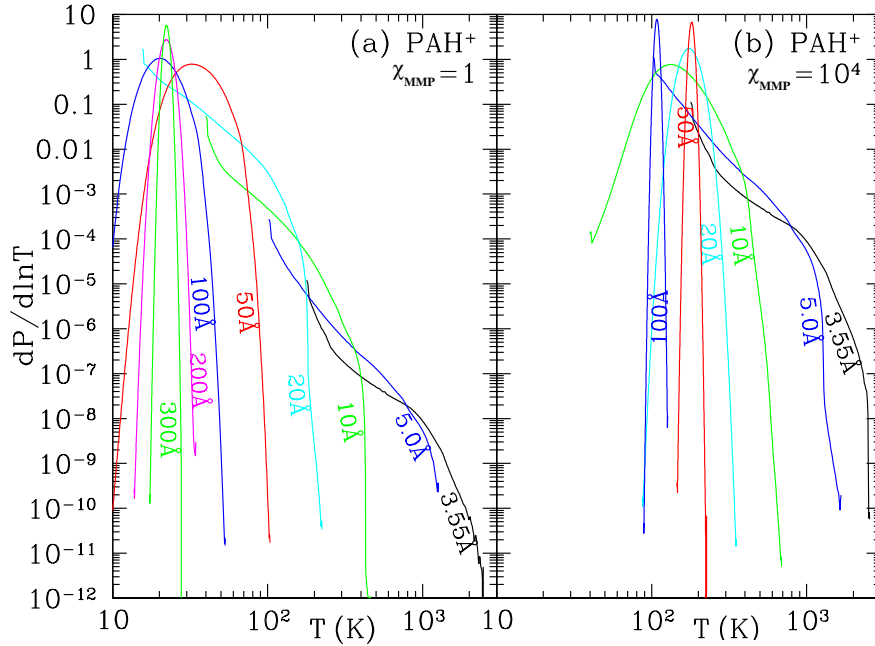


Fig. 12. Temperature probability distribution $dP/d\ln T$ for selected PAH ions heated by starlight with $\chi_{\text{MMP}} = 1$ and $\chi_{\text{MMP}} = 10^4$ (in unit of the MMP local interstellar radiation field). It is interesting to note that in the case of $\chi_{\text{MMP}} = 1$, the $a = 20$ nm grain and the $a = 30$ nm grain (even the $a = 10$ nm grain as well) peak at the same temperature (which is their equilibrium temperature). This is expected from their Rayleigh scattering nature (see the caption of Figure 3). However, in the case of $\chi_{\text{MMP}} = 10^4$, the $a = 5$ nm grain and the $a = 10$ nm grain do not peak at the same temperature, although they both attain equilibrium temperatures. This is because they were “designed” to have different optical properties: PAHs with $a \gtrsim 10$ nm have graphitic properties, while those with $a \lesssim 5$ nm have PAH properties (see Li & Draine 2001a). Taken from Draine & Li (2007).

Whether a grain will undergo stochastic heating depends on (i) the grain size, (ii) the optical properties of the dust, (iii) the thermal properties (e.g. Debye temperature) of the dust, (iv) the starlight intensity, and (v) the hardness of the starlight, which measures the relative amount of short-wavelength (“hard”) photons compared to long-wavelength (“soft”) photons. For a *smaller* grain with a *smaller* UV/visible absorptivity and a *larger* Debye temperature Θ , exposed to starlight of a *lower* intensity and a *harder* spectrum, it is *more* likely for this grain to be stochastically heated by single photons. This is because (i) the specific heat of a grain (at a given temperature) is proportional to a^3/Θ^3 , a single photon (of a given energy) would therefore result in a *more* prominent temperature spike for a *smaller* grain with a *larger* Θ ; (ii) the photon absorption rate is proportional to the starlight intensity and the absorptivity of the dust in the UV/visible wavelength range, a *smaller* grain with a *smaller* UV/visible absorptivity when exposed to a more *dilute* radiation field will have a *smaller* photon absorption rate and will therefore more likely undergo

stochastic heating; (iii) a *more* energetic photon would cause a grain to gain a *larger* temperature raise, grains are therefore *more* likely to experience transient heating when exposed to a *harder* radiation field.

Acknowledgements We thank M. Köhler for her great help in preparing for Figures 9, 11. We thank B.T. Draine, J. Gao, B.W. Jiang, S. Kwok and N. Meyer-Vernet for their helpful comments and suggestions. We also thank A.N. Witt and U.P. Vijh for providing us the ERE data of NGC 7023, F. Banhart and T.J. Bernatowicz respectively for providing us the TEM images of presolar nanodiamonds and presolar graphite with TiC nanocrystals embedded. A.L. is supported in part by a NSF grant (AST-1109039) and a NASA Herschel Theory program.

References

1. Allamandola, L. J., Tielens, A. G. G. M., & Barker, J. R. 1985, *Polycyclic Aromatic Hydrocarbons and the Unidentified Infrared Emission Bands — Auto Exhaust along the Milky Way*, *Astrophys. J. Lett.* **290**, L25
2. Andriesse, C. D., & de Vries, J. S. 1976, *Infrared Observations of M17S at Medium Spatial and Spectral Resolution*, *Astron. Astrophys.* **46**, 143
3. Andriesse, C. D. 1978, *Platt Particles in M 17*, *Astron. Astrophys.* **66**, 169
4. Arendt, R. G., et al. 1998, *The COBE Diffuse Infrared Background Experiment Search for the Cosmic Infrared Background. III. Separation of Galactic Emission from the Infrared Sky Brightness*, *Astrophys. J.* **508**, 74
5. Asplund, M., Grevesse, N., Sauval, A. J., & Scott, P. 2009, *The Chemical Composition of the Sun*, *Ann. Rev. Astron. Astrophys.* **47**, 481
6. Bakes, E. L. O., & Tielens, A. G. G. M. 1994, *The Photoelectric Heating Mechanism for Very Small Graphitic Grains and Polycyclic Aromatic Hydrocarbons*, *Astrophys. J.* **427**, 822
7. Banhart, F., Lyutovich, Y., Braatz, A., Henning, Th., Dorschner, J., & Ott, U. 1998, *Presolar Diamond in Unprocessed Allende Meteorite*, *Meteor. Planet. Sci.* **33**, A12
8. Bernatowicz, T. J., Amari, S., Zinner, E. K., & Lewis, R. S. 1991, *Interstellar Grains within Interstellar Grains*, *Astrophys. J. Lett.* **373**, L73
9. Berné, O., Joblin, C., Rapacioli, M., Thomas, J., Cuillandre, J.-C., & Deville, Y. 2008, *Extended Red Emission and the Evolution of Carbonaceous Nanograins in NGC 7023*, *Astron. Astrophys.* **479**, L41
10. Boulanger, F., & Perault, M. 1988, *Diffuse Infrared Emission from the Galaxy. I. Solar Neighborhood*, *Astrophys. J.* **330**, 964
11. Calzetti, D., Kinney, A. L., & Storchi-Bergmann, T. 1994, *Dust Extinction of the Stellar Continua in Starburst Galaxies: The Ultraviolet and Optical Extinction Law*, *Astrophys. J.* **429**, 582
12. Cardelli, J. A., Clayton, G. C., & Mathis, J. S. 1989, *The Relationship between Infrared, Optical, and Ultraviolet Extinction*, *Astrophys. J.* **345**, 245
13. Casassus, S., Cabrera, G. F., Förster, F., Pearson, T. J., Readhead, A. C. S., & Dickinson, C. 2006, *Morphological Analysis of the Centimeter-Wave Continuum in the Dark Cloud LDN 1622*, *Astrophys. J.* **639**, 951
14. Chang, H.-C., Chen, K., & Kwok, S. 2006, *Nanodiamond as a Possible Carrier of Extended Red Emission*, *Astrophys. J. Lett.* **639**, L63

15. Chigai, T., Yamamoto, T., Kaito, C., & Kimura, Y. 2003, *Are TiC Grains a Carrier of the 21 μ m Emission Band Observed around Post-Asymptotic Giant Branch Objects?* *Astrophys. J.* **587**, 771
16. Darbon, S., Perrin, J.-M., & Sivan, J.-P. 1999, *Observational Constraints on the ERE Interpretation*, *Astron. Astrophys.* **348**, 990
17. Désert, F.-X., Boulanger, F., & Puget, J. L. 1990, *Interstellar Dust Models for Extinction and Emission*, *Astron. Astrophys.* **237**, 215
18. Draine, B.T. 1999, *Diffuse Galactic Emission from Dust Grains*, in Proc. of the EC-TMR Conf. on 3K Cosmology, ed. L. Maiani, F. Melchiorri, & N. Vittorio (Woodbury: AIP), 283
19. Draine, B. T. 2003, *Interstellar Dust Grains*, *Ann. Rev. Astron. Astrophys.* **41**, 241
20. Draine, B. T. 2006, *Can Dust Explain Variations in the D/H Ratio?* in ASP Conf. Ser. **348**, *Astrophysics in the Far Ultraviolet: Five Years of Discovery with FUSE*, ed. G. Sonneborn, H. W. Moos, & B.-G. Andersson (San Francisco: ASP), 58
21. Draine, B.T., & Lee, H.M. 1984, *Optical Properties of Interstellar Graphite and Silicate Grains*, *Astrophys. J.* **285**, 89
22. Draine, B. T., & Anderson, N. 1985, *Temperature Fluctuations and Infrared Emission from Interstellar Grains*, *Astrophys. J.* **292**, 494
23. Draine, B. T., & Lazarian, A. 1998, *Diffuse Galactic Emission from Spinning Dust Grains*, *Astrophys. J. Lett.* **494**, L19
24. Draine, B. T., & Lazarian, A. 1999, *Magnetic Dipole Microwave Emission from Dust Grains*, *Astrophys. J.* **512**, 740
25. Draine, B. T., & Li, A. 2001, *Infrared Emission from Interstellar Dust. I. Stochastic Heating of Small Grains*, *Astrophys. J.* **551**, 807
26. Draine, B. T., & Li, A. 2007, *Infrared Emission from Interstellar Dust. IV. The Silicate-Graphite-PAH Model in the Post-Spitzer Era*, *Astrophys. J.* **657**, 810
27. Dwek, E., et al. 1997, *Detection and Characterization of Cold Interstellar Dust and Polycyclic Aromatic Hydrocarbon Emission from COBE Observations*, *Astrophys. J.* **475**, 565
28. Elíasdóttir, Á., et al. 2009, *Dust Extinction in High-z Galaxies with Gamma-Ray Burst Afterglow Spectroscopy: The 2175 Å Feature at z = 2.45*, *Astrophys. J.* **697**, 1725
29. Finkbeiner, D. P., Davis, M., & Schlegel, D. J. 1999, *Extrapolation of Galactic Dust Emission at 100 μ m to Cosmic Microwave Background Radiation Frequencies Using FIRAS*, *Astrophys. J.* **524**, 867
30. Godard, M., & Dartois, E. 2010, *Photoluminescence of Hydrogenated Amorphous Carbons: Wavelength-Dependent Yield and Implications for the Extended Red Emission*, *Astron. Astrophys.* **519**, A39
31. Gordon, K. D., & Clayton, G. C. 1998, *Starburst-like Dust Extinction in the Small Magellanic Cloud*, *Astrophys. J.* **500**, 816
32. Gordon, K. D., Witt, A. N., & Friedmann, B. C. 1998, *Detection of Extended Red Emission in the Diffuse Interstellar Medium*, *Astrophys. J.* **498**, 522
33. Greenberg, J. M. 1968, *Interstellar Grains*, in *Nebulae and Interstellar Matter*, ed. B. M. Middlehurst & L. H. Aller (Chicago: Univ. of Chicago Press), 221
34. Guillois, O., Ledoux, G., & Reynaud, C. 1999, *Diamond Infrared Emission Bands in Circumstellar Media*, *Astrophys. J. Lett.* **521**, L133

35. Habart, E., Verstraete, L., Boulanger, F., Pineau des Forêts, G., Le Peintre, F., & Bernard, J. P. 2001, *Photoelectric Effect on Dust Grains across the L1721 Cloud in the ρ Ophiuchi Molecular Complex*, *Astron. Astrophys.* **373**, 702
36. Habbal, S.R., et al. 2003 *On the Detection of the Signature of Silicon Nanoparticle Dust Grains in Coronal Holes*, *Astrophys. J.* **592**, L87
37. Helou, G., Malhotra, S., Hollenbach, D. J., Dale, D. A., & Contursi, A. 2001, *Evidence for the Heating of Atomic Interstellar Gas by Polycyclic Aromatic Hydrocarbons*, *Astrophys. J. Lett.* **548**, L73
38. Hoang, T., Draine, B. T., & Lazarian, A. 2010, *Improving the Model of Emission from Spinning Dust: Effects of Grain Wobbling and Transient Spin-up*, *Astrophys. J.* **715**, 1462
39. Hony, S., Tielens, A. G. G. M., Waters, L. B. F. M., & de Koter, A. 2003, *The Circumstellar Envelope of the C-rich Post-AGB Star HD 56126*, *Astron. Astrophys.* **402**, 211
40. Jones, A. P., & d'Hendecourt, L. 2000, *Interstellar Nanodiamonds: the Carriers of Mid-Infrared Emission Bands?* *Astron. Astrophys.* **355**, 1191
41. Kapteyn, J. C. 1904, *Remarks on the Determination of the Number and Mean Parallax of Stars of Different Magnitude and the Absorption of Light in Space*, *Astron. J.* **24**, 115
42. Kwok, S., Volk, K. M., & Hrivnak, B. J. 1989, *A 21 μ m Emission Feature in Four Proto-Planetary Nebulae*, *Astrophys. J. Lett.* **345**, L51
43. Ledoux, G., et al. 1998, *Silicon as a Candidate Carrier for ERE*, *Astron. Astrophys.* **333**, L39
44. Léger, A., & Puget, J. L. 1984, *Identification of the 'Unidentified' IR Emission Features of Interstellar Dust?* *Astron. Astrophys.* **137**, L5
45. Leinert, C., Bowyer, S., Haikala, L.K., Hanner, M.S., Hauser, M.G., Levasseur-Regourd, A.-C., Mann, I., Mattila, K., Reach, W.T., Schlosser, W., Staude, H.J., Toller, G.N., Weiland, J.L., Weinberg, J.L., and Witt, A.N.: 1998, *Astronomy and Astrophysics Supplement Series* **127**, 1.
46. Lewis, R. S., Ming, T., Wacker, J. F., Anders, E., & Steel, E. 1987, *Interstellar Diamonds in Meteorites*, *Nature* **326**, 160
47. Li, A. 2003, *On TiC Nanoparticles as the Origin of the 21 μ m Emission Feature in Post-Asymptotic Giant Branch Stars*, *Astrophys. J.* **599**, L45
48. Li, A. 2004, *Interaction of Nanoparticles with Radiation*, in ASP Conf. Ser. **309**, *Astrophysics of Dust*, ed. A. N. Witt, G. C. Clayton, & B. T. Draine (San Francisco: ASP), 417
49. Li, A., & Draine, B. T. 2001a, *Infrared Emission from Interstellar Dust. II. The Diffuse Interstellar Medium*, *Astrophys. J.* **554**, 778
50. Li, A., & Draine, B. T. 2001b, *On Ultrasmall Silicate Grains in the Diffuse Interstellar Medium*, *Astrophys. J. Lett.* **550**, L213
51. Li, A., & Draine, B.T. 2002, *Are Silicon Nanoparticles an Interstellar Dust Component?* *Astrophys. J.* **564**, 803
52. Liang, S. L., & Li, A. 2010, *Probing Extragalactic Dust through Nearby Gamma-ray Burst Afterglows*, *Astrophys. J.* **710**, 648
53. Lodders, K. 2005, *Presolar Grains from Meteorites: Remnants from the Early Times of the Solar System*, *Chemie der Erde/Geochemistry* **65**, 93
54. Lutz, D., Valiante, E., Sturm, E., Genzel, R., Tacconi, L. J., Lehnert, M. D., Sternberg, A., & Baker, A. J. 2005, *Mid-Infrared Spectroscopy of Two Luminous Submillimeter Galaxies at $z \sim 2.8$* , *Astrophys. J. Lett.* **625**, L83

55. Mann, I. 2007, *Nanoparticles in the Inner Solar System*, Planet. Space Sci. **55**, 1000
56. Mann, I. 2010, *Interstellar Dust in the Solar System*, Ann. Rev. Astron. Astrophys. **48**, 173
57. Mann, I., & Murad, E. 2005, *On the Existence of Silicon Nanodust near the Sun*, Astrophys. J. Lett. **624**, L125
58. Mathis, J. S., Rumpl, W., & Nordsieck, K. H. 1977, *The Size Distribution of Interstellar Grains*, Astrophys. J. **217**, 425
59. Mathis, J. S., Mezger, P. G., & Panagia, N. 1983, *Interstellar Radiation Field and Dust Temperatures in the Diffuse Interstellar Matter and in Giant Molecular Clouds*, Astron. Astrophys. **128**, 212
60. Mattila, K., Lemke, D., Haikala, L. K., Laureijs, R. J., Léger, A., Lehtinen, K., Leinert, C., & Mezger, P. G. 1996, *Spectrophotometry of UIR Bands in the Diffuse Emission of the Galactic Disk*, Astron. Astrophys. **315**, L353
61. Noll, S., et al. 2009, *GMASS Ultra-Deep Spectroscopy of Galaxies at $z \sim 2$. IV. The Variety of Dust Populations*, Astron. Astrophys. **499**, 69
62. Onaka, T., Yamamura, I., Tanabe, T., Roellig, T. L., & Yuen, L. 1996, *Detection of the Mid-Infrared Unidentified Bands in the Diffuse Galactic Emission by IRTS*, Publ. Astron. Soc. Japan **48**, L59
63. Ott, U. 2007, *Presolar Grains in Meteorites and Their Compositions*, Space Sci. Rev. **130**, 87
64. Planck Collaboration, et al. 2011, *Planck Early Results XX: New Light on Anomalous Microwave Emission from Spinning Dust Grains*, Astron. Astrophys., in press (arXiv:1101.2031)
65. Platt, J. R. 1956, *On the Optical Properties of Interstellar Dust*, Astrophys. J. **123**, 486
66. Posch, T., Mutschke, H., & Andersen, A. 2004, *Reconsidering the Origin of the 21 μm Feature: Oxides in Carbon-rich Protoplanetary Nebulae?* Astrophys. J. **616**, 1167
67. Prochaska, J. X., et al. 2009, *The First Positive Detection of Molecular Gas in a GRB Host Galaxy*, Astrophys. J. **691**, 27
68. Purcell, E.M. 1969, *On the Absorption and Emission of Light by Interstellar Grains*, Astrophys. J. **158**, 433
69. Rudnick, J. 1936, *On the Reddening in B-Type Stars*, Astrophys. J. **83**, 394
70. Seahra, S. S., & Duley, W. W. 1999, *Extended Red Emission from Carbon Clusters in Interstellar Clouds*, Astrophys. J. **520**, 719
71. Sellgren, K., Werner, M. W., & Dinerstein, H. L. 1983, *Extended Near-Infrared Emission from Visual Reflection Nebulae*, Astrophys. J. Lett. **271**, L13
72. Sellgren, K. 1984, *The Near-Infrared Continuum Emission of Visual Reflection Nebulae*, Astrophys. J. **277**, 623
73. Siebenmorgen, R., & Kruegel, E. 1992, *Dust Model Containing Polycyclic Aromatic Hydrocarbons in Various Environments*, Astron. Astrophys. **259**, 614
74. Smith, J. D. T., et al. 2007, *The Mid-Infrared Spectrum of Star-forming Galaxies: Global Properties of Polycyclic Aromatic Hydrocarbon Emission*, Astrophys. J. **656**, 770
75. Smith, T. L., & Witt, A. N. 2002, *The Photophysics of the Carrier of Extended Red Emission*, Astrophys. J. **565**, 304
76. Stebbins, J., Huffer, C. M., & Whitford, A. E. 1939, *Space Reddening in the Galaxy*, Astrophys. J. **90**, 209

77. Szomoru, A., & Guhathakurta, P. 1998, *Optical Spectroscopy of Galactic Cirrus Clouds: Extended Red Emission in the Diffuse Interstellar Medium*, *Astrophys. J. Lett.* **494**, L93
78. Tanaka, M., Matsumoto, T., Murakami, H., Kawada, M., Noda, M., & Matsumura, S. 1996, *IRTS Observation of the Unidentified 3.3 μm Band in the Diffuse Galactic Emission*, *Publ. Astron. Soc. Japan* **48**, L53
79. Tielens, A. G. G. M., Hony, S., van Kerckhoven, C., & Peeters, E. 1999, *Interstellar and Circumstellar PAHs*, in *ESA SP-427, The Universe as Seen by ISO*, ed. P. Cox & M. F. Kessler (Noordwijk: ESA), 579
80. Tielens, A. G. G. M. 2008, *Interstellar Polycyclic Aromatic Hydrocarbon Molecules*, *Ann. Rev. Astron. Astrophys.* **46**, 289
81. Trumpler, R. J. 1930, *Absorption of Light in the Galactic System*, *Publ. Astro. Soc. Pacific* **42**, 214
82. van Kerckhoven, C., Tielens, A. G. G. M., & Waelkens, C. 2002, *Nanodiamonds around HD 97048 and Elias 1*, *Astron. Astrophys.* **384**, 568
83. Vidal, M., et al. 2011, *Dust-Correlated CM Wavelength Continuum Emission from Translucent Clouds ζ Oph and LDN 1780*, *Mon. Not. Roy. Astron. Soc.* **516**, in press
84. Vijh, U. P., Witt, A. N., & Gordon, K. D. 2004, *Discovery of Blue Luminescence in the Red Rectangle: Possible Fluorescence from Neutral Polycyclic Aromatic Hydrocarbon Molecules?* *Astrophys. J.* **606**, L65
85. Vijh, U. P., Witt, A. N., & Gordon, K. D. 2005, *Blue Luminescence and the Presence of Small Polycyclic Aromatic Hydrocarbons in the Interstellar Medium*, *Astrophys. J.* **633**, 262
86. Vijh, U. P., Witt, A. N., York, D. G., Dwarkadas, V. V., Woodgate, B. E., & Palunas, P. 2006, *Optical Emission Band Morphologies of the Red Rectangle*, *Astrophys. J.* **653**, 1336
87. von Helden, G., Tielens, A. G. G. M., van Heijnsbergen, D., Duncan, M. A., Hony, S., Waters, L. B. F. M., & Meijer, G. 2000, *Titanium Carbide Nanocrystals in Circumstellar Environments*, *Science* **288**, 313
88. Wada, S., Mizutani, Y., Narisawa, T., & Tokunaga, A. T. 2009, *On the Carrier of the Extended Red Emission and Blue Luminescence*, *Astrophys. J.* **690**, 111
89. Watson, W. D. 1972, *Heating of Interstellar HI Clouds by Ultraviolet Photoelectron Emission from Grains*, *Astrophys. J.* **176**, 103
90. Weiland, J. L., Blitz, L., Dwek, E., Hauser, M. G., Magnani, L., & Rickard, L. J. 1986, *Infrared Cirrus and High-Latitude Molecular Clouds*, *Astrophys. J. Lett.* **306**, L101
91. Weingartner, J. C., & Draine, B. T. 2001a, *Dust Grain-Size Distributions and Extinction in the Milky Way, Large Magellanic Cloud, and Small Magellanic Cloud*, *Astrophys. J.* **548**, 296
92. Weingartner, J. C., & Draine, B. T. 2001b, *Photoelectric Emission from Interstellar Dust: Grain Charging and Gas Heating*, *Astrophys. J. Suppl. Ser.* **134**, 263
93. Witt, A.N., Gordon, K.D., & Furton, D.G. 1998, *Silicon Nanoparticles: Source of Extended Red Emission?* *Astrophys. J.* **501**, L111
94. Witt, A. N., & Vijh, U. P. 2004, *Extended Red Emission: Photoluminescence by Interstellar Nanoparticles*, in *ASP Conf. Ser.* **309**, *Astrophysics of Dust*, ed. A. N. Witt, G. C. Clayton, & B. T. Draine (San Francisco: ASP), 115

95. Witt, A. N., Gordon, K. D., Vijn, U. P., Sell, P. H., Smith, T. L., & Xie, R.-H. 2006, *The Excitation of Extended Red Emission: New Constraints on its Carrier from Hubble Space Telescope Observations of NGC 7023*, *Astrophys. J.* **636**, 303
96. Xiang, F. Y., Li, A., & Zhong, J. X. 2011, *A Tale of Two Mysteries in Interstellar Astrophysics: The 2175 Å Extinction Bump and Diffuse Interstellar Bands*, *Astrophys. J.* **733**, 91
97. Yan, L., et al. 2005, *Spitzer Detection of Polycyclic Aromatic Hydrocarbon and Silicate Dust Features in the Mid-Infrared Spectra of $z \sim 2$ Ultraluminous Infrared Galaxies*, *Astrophys. J.* **628**, 604
98. Ysard, N., Miville-Deschênes, M. A., & Verstraete, L. 2010, *Probing the Origin of the Microwave Anomalous Foreground*, *Astron. Astrophys.* **509**, L1
99. Zhang, K., Jiang, B. W., & Li, A. 2009, *On the Carriers of the 21 μm Emission Feature in Post-Asymptotic Giant Branch Stars*, *Mon. Not. Roy. Astron. Soc.* **396**, 1247